AGU PUBLICATIONS

Geophysical Research Letters

RESEARCH LETTER
10.1002/2014GL060306

Key Points:
- The magnitude −7 level earthquakes are identified in a laboratory experiment
- Ruptures from kilometer to millimeter scale satisfy the same self-similar relationship
- Broadband recording of AE events under a triaxial condition has been succeeded

Supporting Information:
- Readme
- Figure S1
- Figure S2
- Table S1

Correspondence to:
N. Yoshimitsu,
ynana@eri.u-tokyo.ac.jp

Citation:
Yoshimitsu, N., H. Kawakata, and N. Takahashi (2014), Magnitude −7 level earthquakes: A new lower limit of self-similarity in seismic scaling relationships, *Geophys. Res. Lett.*, *41*, 4495–4502, doi:10.1002/2014GL060306.

Received 21 APR 2014
Accepted 5 JUN 2014
Accepted article online 9 JUN 2014
Published online 3 JUL 2014

Magnitude −7 level earthquakes: A new lower limit of self-similarity in seismic scaling relationships

Nana Yoshimitsu[1,2], Hironori Kawakata[3], and Naoki Takahashi[4]

[1]The Center for Integrated Disaster Information Research, Earthquake Research Institute, University of Tokyo, Tokyo, Japan, [2]Earthquake Research Institute, University of Tokyo, Tokyo, Japan, [3]College of Science and Engineering, Ritsumeikan University, Shiga, Japan, [4]Sumitomo Mitsui Construction Co., Ltd., Tokyo, Japan

Abstract Microfractures occurring in a rock sample that are called acoustic emission (AE) events show some similar features to earthquakes. However, it remains to be shown whether or not AE equate to ultramicroearthquakes. In this study, we show the existence of magnitude −7 level earthquakes based on seismological analyses of AE source parameters. Advances in multichannel, broadband, high-speed continuous recording of AE under seismogenic pressure conditions has facilitated increasingly robust measurement. Source parameters of AE show that AE events satisfy the same scaling relationship as natural earthquakes in which seismic moment is inversely proportional to the cube of corner frequency. This result suggests that both millimeter scale fractures and natural earthquakes of kilometer scale ruptures are highly similar as physical processes. Hence, AE events can be interpreted as ultramicroearthquakes having a magnitude of about −7. These results demonstrate that laboratory observation is an effective approach in studying natural earthquake generation process.

1. Introduction

Rock fracture experiments offer highly effective tool for simulating fine-scale faulting processes. Hypocenter localization and AE migration in fracturing samples resemble fault development processes [*Yanagidani et al.*, 1985; *Lockner et al.*, 1991]. Although AE events seem to be a good simulation of actual earthquake events [*Scholz*, 1968a; *Lei et al.*, 2000], researchers should be careful to directly apply knowledge obtained in the laboratory for natural field because there was a large-scale gap. In order to demonstrate similarities between AE and natural large-scale ruptures, we estimated the source parameters of seismic moment (M_0) and corner frequency (f_c), which represent the magnitude and the inverse of the characteristic source time of a given seismic event, respectively. Earthquakes having a moment magnitude (M_w) of −4 to 8 satisfy the scaling relationship of $M_0 \propto f_c^{-3}$ [*Aki*, 1967; *Abercrombie*, 1995; *Hiramatsu et al.*, 2002; *Prieto et al.*, 2004; *Yamada et al.*, 2007; *Kwiatek et al.*, 2011]. Recently, some attempts are made to show that the similar relationship can be applied to larger earthquakes [*Allmann and Shearer*, 2009; *Convers and Newman*, 2011]. For smaller AE events, limited sensitivity of transducer elements has precluded previous lab-based determination of source parameters. Prevalent resonant-type transducers (e.g., $Pb[Zr,Ti]O_3$; PZT) record a relatively narrow or limited frequency band, with poor damping. These factors confined their use primarily to detection of wave amplitudes and traveltimes and keep away from seismological frequency analyses [*Mogi*, 1962; *Scholz*, 1968b]. Researchers recently demonstrated broadband recording of transmitted waveforms under triaxial conditions using metallic vessels to shield broadband transducers from the confining pressure [*Yoshimitsu et al.*, 2009; *Kawakata et al.*, 2011]. Building on these advances, this study used a small, lightweight, hermetically sealed titanium casing to protect the transducer. Coupling these protection cases with small, broadband transducers allowed multichannel, broadband recording of AE events. The advanced experimental system could thus address the question of whether AE source parameters behave as ultramicroearthquakes.

2. Methods

2.1. Experimental Procedures

The rock sample used in the fracture experiment was cylindrical Westerly granite having a diameter of 49.53 ± 0.04 mm and a height of 100.24 mm. The grain size of Westerly granite ranges from about

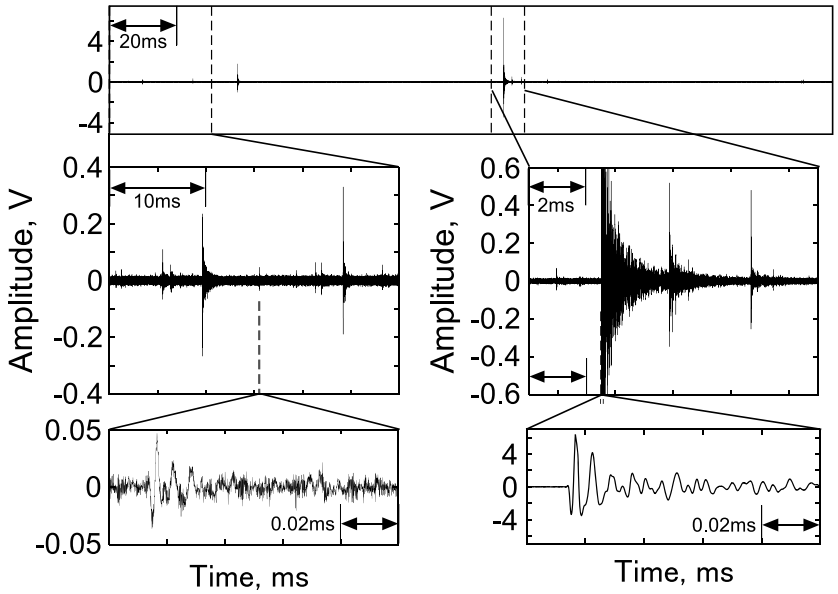

Figure 1. An example of (top) the continuous record for 209.7152 ms in a long time window, (middle) an enlarged view for 30 ms, and (bottom) a further enlarged view for 0.1 ms.

0.05 to 2.20 mm. Seven positions were polished by a grinder on the sample circumferential surface in order to mount the titanium cases containing specially manufactured broadband transducers custom-made by Fuji Ceramics Corporation (5145SMAT-1152). The cases were directly glued to the surfaces using a compound resin. The contact face of each transducer was 6 mm in diameter, while each assembly case was 11 mm in diameter. All transducers could accurately record frequencies from 100 kHz to 2000 kHz. The sample was sheathed in heat-shrink silicone rubber tubing to protect it from the confining oil. The transducers were covered with liquid silicone rubber. Loading was performed at an ambient temperature under a confining pressure of 10 MPa. We used a circumferential displacement loading rate [*Kawakata et al.*, 1999] of 74.12 μm/s in order to attain gradual development of a rupture plane. Signals from each channel were continuously recorded at 20 Msps throughout the loading process, and data were transferred to RAID (redundant array of inexpensive disks) every 2^{20} samples per channel. Loading control was maintained for 5 h, 53 min and 53 s, by which point the sample experienced ~46 MPa stress decrease after the peak stress (296 MPa). The sample did not fully fracture, but the edge of a fault plane appeared on the surface of the recovered sample.

2.2. Event Detection and Location

As shown in Figure 1, numerous events of varying amplitudes appeared in continuous waveforms recorded at every channel. We used an Akaike information criteria algorithm [*Akaike*, 1973; *Takanami and Kitagawa*, 1988] to identify events within the continuous data. Least squares methods were used to estimate a total of 6794 hypocenters from the arrival time list. We arranged six wave paths from wave transmission tests conducted prior to loading experiments to estimate a *P* wave velocity of 5700 m/s for the sample. Event rates sharply increased immediately following the peak stress and 15 min after the peak stress as shown in Figure 2. Hypocenter distributions from these two periods were imaged within the recovered sample using X-ray computer tomography (CT). The CT image revealed a clear rupture plane in the sample (Figure 3). Event activity initially concentrated near the surface and then gradually migrates toward the center of the sample. These periods correspond to stages when differential stress rapidly decreased and gave rise to the AE events analyzed for seismic parameters. The two event sequences were obtained from data files DataDD0008 and DataFF0000, which contained waveform records approximately 3 min in durations. We defined clusters as events having hypocenters within 2 mm radius and correlation coefficients in excess of 0.80 for four or more channels. This clustering procedure is equivalent to the procedure used to detect repeating earthquakes [*Nadeau and Johnson*, 1998; *Igarashi et al.*, 2003]. Identical hypocenters for each cluster allowed us to assume

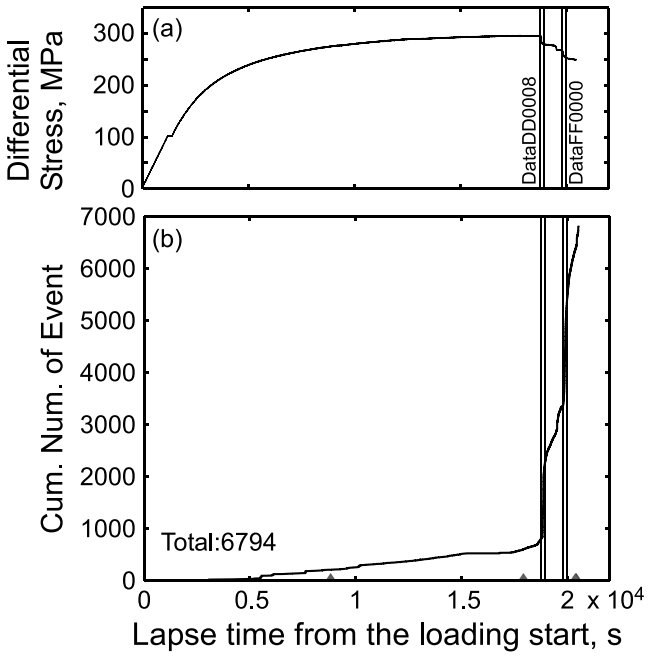

Figure 2. (a) Temporal changes in differential stress and (b) cumulative number of events. Triangular marks in Figure 2 (bottom) indicate short periods of missing data.

a constant attenuation factor in each cluster for each transducer. The largest clusters in DataDD0008 and DataFF0000 were referred to as the D- and F-clusters, included 142 and 913 events, respectively. Centroid locations for each cluster are shown in Figure 3. The difference in event origin times for these two clusters was about 15 min. The polarities of the initial wave motions show both positive and negative at channel for the events belonging to the D- and F-clusters. The fact indicates that the clusters did not consist of open crack-type events but shear-type events.

2.3. Calibration

Events in waveform records obtained from a transducer have a unit of voltage, and they are subject to the transducer's sensitivity. Calculation of displacement spectrum therefore required calibration of the transducer. We applied a deconvolution technique to calibrate broadband transducers. Prior to loading, we affixed a broadband transducer to the middle region of the sample's side. We then applied a step voltage to the transducer and measured vibration of the opposing sample surface by a laser Doppler vibrometer (Figure S1a in the supporting information). The laser Doppler vibrometer can record surface vibration as a velocity waveform with a flat sensitivity from DC to 6 MHz [*Nishizawa et al.*, 1997]. We also measured surface vibrations as a voltage waveform by the broadband transducer used in the triaxial experiment (Figure S1b). Fourier transformation is performed for these velocity and voltage waveforms, and spectra were obtained. Then, we obtained the transducer's sensitivity function from the spectral ratio of these spectra. The unit of the sensitivity function is V/(m/s), as shown in Figure S1c.

2.4. Estimation of Seismic Parameters

We analyzed waveforms within a 102.4 μs time window occurring 2.5 μs before *S* wave arrival. Since *S* wave onsets are unclear in the record, we calculated theoretical *S* wave arrival times with an *S* wave velocity (V_s) as given by the equation, $V_s = V_p/1.73$, where V_p is *P* wave velocity. We obtained displacement spectra from the time integral of the spectra corrected by deconvolution with the estimated sensitivity function. The *S* wave displacement spectrum *U* is generally modeled as follows:

$$U(f) = \Omega_0 e^{-(\pi f t/Q)} / [1 + (f/f_c)^{\gamma n}]^{1/\gamma}, \quad (1)$$

where Ω_0 is the long period amplitude, *f* the frequency, f_c the corner frequency of the *S* wave spectrum, *t* the traveltime, *Q* the quality factor, *n* the high-frequency falloff rate, and γ a constant that controls the sharpness of the spectrum corner. The *n* and γ terms were set to 2 and 10, respectively, according to the shape of displacement spectra.

In order to estimate the signal-to-noise ratio (S/N ratio), we calculated the spectrum of a typical noise waveform (2048 samples) without any signal-like features for each cluster at each channel. We considered a low S/N ratio to be one for which the mean of the signal spectra relative to noise for every 100 kHz was lower than two. Waveforms with low S/N ratio between 100 kHz and 1000 kHz were excluded from further analysis. We selected an upper frequency range limit of 2000 kHz. For waveforms with low S/N ratio between 1000 kHz and 2000 kHz, we lowered the upper limit to the minimum frequency at which S/N was lower than two in the target frequency band.

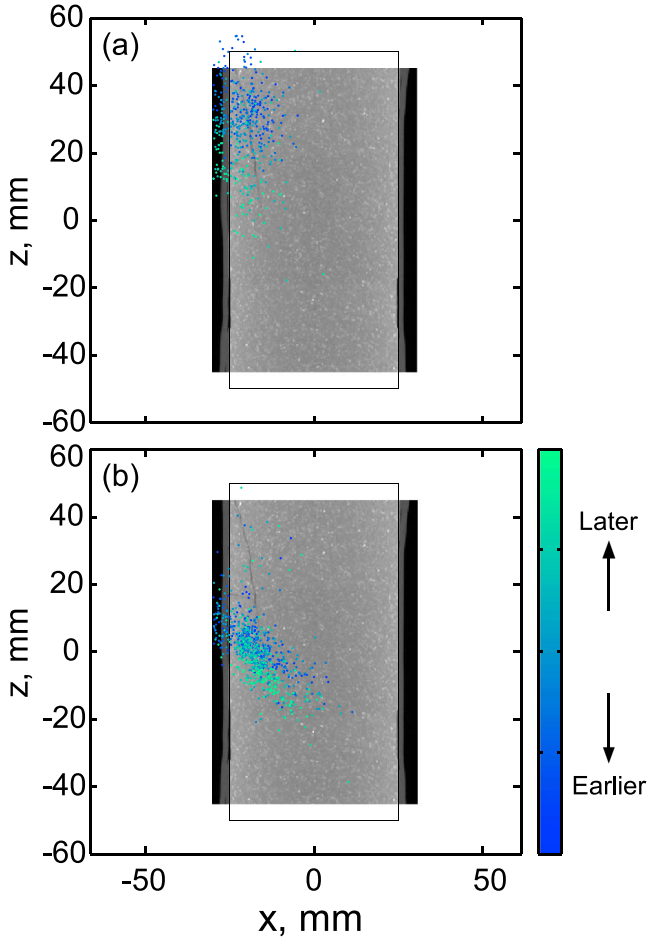

Figure 3. Vertical cross-section images of the sample obtained by X-ray CT scan (including cylindrical axis), overlaid with the hypocenters of (a) the D-cluster and (b) the F-cluster. Blue circles indicate earlier events, and green circles indicate later events in each cluster.

If we estimated f_c and Q values from a spectrum all together, the trade-offs between f_c and Q values could arise. To check this issue from the fitting residual, we perform a grid search of Q values from 10 to 300 over intervals of 10 and of f_c from 100 kHz to 1000 kHz over 50 kHz intervals with the estimated Ω_0. For a large number of waveforms, there were only small trade-off effects. The other small number of waveforms that showed significant trade-off effects with nonunique minima was excluded from the further spectral analyses. Finally, the D-cluster contained 120 events, and the F-cluster contained 454 events recorded by four or more waveforms.

Next, we assumed that all events in a cluster had the same attenuation parameter (Q) for each channel due to their identical travel paths. We could then set Q values for each cluster at each channel according to results from the pregrid search for f_c, Ω_0, and Q values. These Q values (Table S1) allowed a second grid search of the displacement spectra to estimate f_c and Ω_0. Search ranges were from 10^{-18} ms to 10^{-15} ms at increment intervals of $10^{0.01}$ ms for Ω_0 and from 100 kHz to the upper frequency limit at a 10 kHz interval for f_c. We excluded results for which estimated Ω_0 or f_c reached the search limit. Seismic moment, M_0, was calculated from Ω_0 according to the following equation

$$M_0 = 4\pi\rho V_s^3 R\left(\Omega_0 / R_{\theta,\phi}\right), \tag{2}$$

where ρ is the density, R the distance between the source and the transducer, and $R_{\theta,\phi}$ the averaged radiation pattern coefficient (0.63 for S waves) [*Aki and Richards*, 1980]. Using M_0 values in the unit of Newton meter, we calculated M_w from the equation:

$$M_w = (\log M_0 - 9.1)/1.5. \tag{3}$$

Figures 4a and 4b show waveforms of a typical event along with their displacement spectra and fitted results.

3. Source Parameters

3.1. Scaling Relationship of Source Parameters

Figure 5 shows M_0 and f_c values estimated from the D-cluster and F-cluster events, along with results from previous studies for comparison [*Urbancic and Young*, 1993; *Abercrombie*, 1995; *Urbancic et al.*, 1996; *Collins and Young*, 2000; *Hiramatsu et al.*, 2002; *Ide et al.*, 2003; *Prieto et al.*, 2004; *Abercrombie and Rice*, 2005; *Oye et al.*, 2005; *Yamada et al.*, 2007; *Domanski and Gibowicz*, 2008; *Kwiatek et al.*, 2010; *Kwiatek et al.*, 2011; *Kwiatek et al.*, 2013; *Somei et al.*, 2014]. In Figures 5b and 5c, M_0 and f_c values are estimated for the D-cluster and

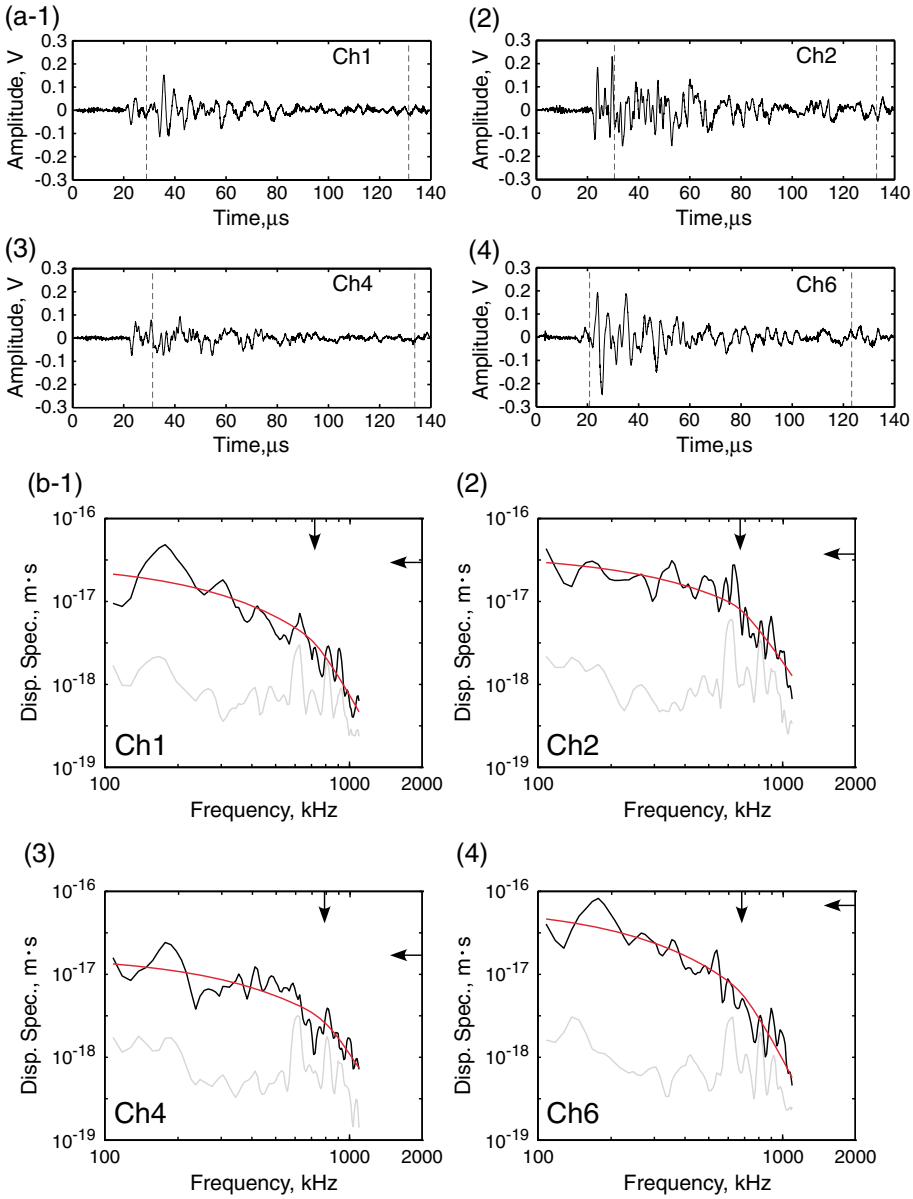

Figure 4. (a) Waveforms of fourteenth event in the F-cluster recorded by Ch1, Ch2, Ch4, and Ch6. We analyzed the 2048 data samples between the dotted lines. The origin time is aligned with time equal to 10 μs. (b) Amplitude spectra of the fourteenth event in the F-cluster recorded by Ch1, Ch2, Ch4, and Ch6. The black depict signal spectra, gray depict noise spectra, and red depict the best fitted. The arrow pointing left indicates the estimated long period amplitude, and the arrow pointing down indicates the estimated corner frequency.

F-cluster events together with error bars. The error bars demonstrate standard deviations of estimated values for all available transducers. The source parameters estimated from our data follow the same scaling relationship as that which applies to natural earthquakes. For the D-cluster, M_0 ranged from 1.67×10^{-3} N m ($M_w = -7.92$) to 2.33×10^{-2} N m ($M_w = -7.15$), and f_c ranged from 270 kHz to 1040 kHz, respectively. Mean estimation error is as small as $\pm 10^{0.15}$ N m for M_0 and $\pm 10^{0.2}$ kHz for f_c. For the F-cluster, M_0 ranged from 9.40×10^{-4} N m ($M_w = -8.08$) to 4.02×10^{-2} N m ($M_w = -7.00$), while f_c ranged from 325 kHz to 1105 kHz. Mean estimation error is as small as $\pm 10^{0.14}$ N m for M_0 and $\pm 10^{0.07}$ kHz for f_c. Neither transition of event size nor corner frequency showed time dependency.

It is worthy of note that the scaling relationship wherein M_0 is inversely proportional to the cube of f_c is defined only from AE events observed in our experiment (Figures 5b and 5c). AE source parameters estimated

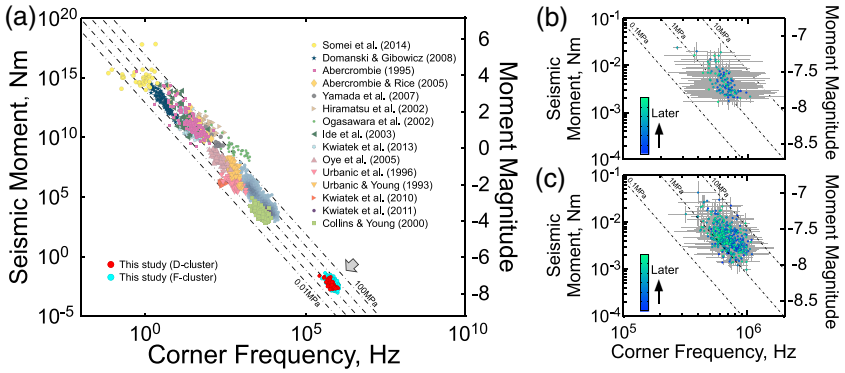

Figure 5. (a) The relationship between M_o and f_c. The parameters estimated from the D-cluster are plotted as red circles, and those estimated from the F-cluster are plotted as light blue circles. The other points are results from previous studies. Dashed dotted lines represent stress drops of 0.1, 1, 10, and 100 MPa from Madariaga's source model. (b) Close-up view of Figure 5a for the D-cluster. The color scale reflects the relative occurrence time within the cluster. Blue denotes earlier events, and green denotes later events. Dashed dotted lines represent stress drops of 0.1, 1, and 10 MPa from Madariaga's source model. (c) Close-up view of Figure 5a for the F-cluster (caption same as for Figure 5b).

in previous experiments using PZT elements as detectors or insufficiently calibrated records collected at atmospheric pressure did not satisfy this cubic relationship [*Sellers et al.*, 2003]. The inconsistencies may arise from insufficient calibration of the transducers especially in the high-frequency range. Low confining pressure could also affect AE processes because open cracking events predominate over shear events under conditions of insufficient confining pressure. To further demonstrate the source parameter relationship of individual AE, we optimized continuous, multichannel recording at the highest possible sampling frequency. Multichannel-triggered recording [*Thompson et al.*, 2006] can only detect events with signals whose amplitudes exceed a preset threshold, though single-channel continuous recording was conducted in tandem. Properly calibrated, our experimental apparatus recorded AE under triaxial conditions that could detect AE whose amplitudes were far below previous empirical thresholds.

3.2. Stress Drop

The stress drop representing the stress difference on a fault plane before and after a natural earthquake is a critical seismic process. Earthquake stress drops usually range from 0.1 MPa to 100 MPa. Assuming the circular crack model, the stress drop ($\Delta\sigma$) can be calculated from source radius r and M_0 as $\Delta\sigma = 7M_0/16r^3$ [*Eshelby*, 1957], where $r = 0.21V_s/f_c$ [*Madariaga*, 1976], assuming S wave velocity, Vs, of 3295 m/s. The stress drop values in this study ranged from 0.4 MPa to 11.8 MPa. In both clusters, stress drop histograms roughly follow lognormal distributions and have similar mean values. As shown in Figure 3, events in the D-cluster and F-cluster occurred within different regions in the fault plane, with the F-cluster located in a lower area. Later events in both clusters occurred concentrated in a lower area of the cluster. Then, all events in two clusters were considered to have occurred along a newly developing fault at that moment. That should be the reason why events in the two clusters exhibited almost the same stress drop values, though they experienced different bulk differential stress.

Source radii of all AE events ranged from 0.6 mm to 2.6 mm, with larger events exhibiting larger source radii. Previous, thin section analysis of a Westerly granite sample subjected to triaxial compression fracture experiments found cracks extending about 0.5 mm along intragranular areas and about 0.6 mm along grain boundary areas [*Moore and Lockner*, 1995]. Thus, smaller source radii events were considered as microfractures in/between grains. Thin section observation also pointed out small cracks in a fracturing rock sample that connected each other to generate large shear rupture. Larger source radii events could be caused by such an interaction of previously generated cracks.

3.3. Self-Similarity of Earthquakes

Self-similarity is a relationship in which phenomena are approximately similar at different scales. In seismology, for example, fault dimension and magnitude are self-similar [*Somerville et al.*, 1999]. The self-similar relationship between M_0 and f_c has received considerable attention due to its potential in translating findings from smaller seismic events to understanding larger earthquakes. A recent study has proposed a new self-similar scaling law

for slow earthquakes [*Ide et al.*, 2007]. Self-similar relationship should be a key to understand the macroscopic phenomena of earthquakes occurrence [*Iio*, 1986]. Questions remain as to the lower limits of self-similarity between M_0 and f_c, however. This study shows that source parameters estimated from AE events adhere to the same scaling relationships that apply to natural earthquakes. AE events arising from microfractures in a rock sample subjected to a confining pressure can thus be interpreted as ultrasmall earthquakes.

Another scaling relationship, the magnitude-frequency distributions for the two clusters are shown in Figure S2. The AE events in these two clusters satisfy the Gutenberg-Richter law. The minimum moment magnitude of completeness (M_{min}) was about −7.8, which is slightly larger than the minimum magnitude of analyzed events. The *b* values estimated with a maximum likelihood estimation function [*Utsu*, 1965] for the D-cluster and F-cluster were 2.3 and 2.0, respectively. Compared to the natural environments, *b* values estimated in this study thus exceed typical values. As shown in Figure 3, both clusters have an extremely high seismic rate in localized areas. The high *b* value is able to be interpreted by a large number of cracks generated in the localized regions [*McNutt*, 2005; *Farrell et al.*, 2009] during the period that spanned the two clusters. It should be kept in mind that this *b* value is estimated from repeating events clusters.

4. Conclusions

Laboratory-based rock fracture experiments allow us to control dynamic fracture and observe the rupture from its inception to arrest, that is, to say the entire life of the rupture. We showed the clear continuity of the self-similar relationship between M_0 and f_c from kilometer-scale natural earthquakes to millimeter-scale ultramicroruptures in a rock sample. This means that laboratory findings can be used to query other natural seismic processes. Experimental observation of patterns in AE mechanism, stress drop, and magnitude during the final stages of a rupture process can shed light on poorly understood phenomenon in seismology, for example, the stopping of mechanism of fault ruptures. In this way, varieties of seismological analytical approaches are applicable to AE records and can be used to deepen our understanding of earthquakes generation.

Acknowledgments

We thank late T. Yanagidani and I. Doi for their helpful comments and discussions regarding this research. J. Takeuchi provided us technical support in setting up the recording system. X-ray CT image was obtained by H. Hirai's help. We thank H. Inaba and Y. Yoshitome for their technical support to develop the new transducers. Comments and suggestions from two anonymous reviewers and Editor A. V. Newman were helpful to improve this paper. This study was supported by the Research Fellowship of the Japan Society for the Promotion of Science for Young Scientists and the Ministry of Education, Culture, Sports, Science and Technology (MEXT) of Japan under its Observation and Research Program for Prediction of Earthquakes and Volcanic Eruptions.

The Editor thanks two anonymous reviewers for their assistance in evaluating this paper.

References

Abercrombie, R. E. (1995), Earthquake source scaling relationships from −1 to 5 M_L using seismograms recorded at 2.5-km depth, *J. Geophys. Res.*, *100*, 24,015–24,036, doi:10.1029/95JB02397.

Abercrombie, R., and J. Rice (2005), Can observations of earthquake scaling constrain slip weakening?, *Geophys. J. Int.*, *162*, 406–424, doi:10.1111/j.1365-246X.2005.02579.x.

Akaike, H. (1973), *Information Theory and an Extension of the Maximum Likelihood Principle*, paper presented at 2nd Int. Symp. Info. Theory, pp. 267–281, Akademia Kiado, Budapest, Hungary.

Aki, K. (1967), Scaling law of seismic spectrum, *J. Geophys. Res.*, *72*(4), 1217–1231, doi:10.1029/JZ072i004p01217.

Aki, K., and P. Richards (1980), *Quantitative Seismology*, W. H. Freeman, New York.

Allmann, B. P., and P. M. Shearer (2009), Global variations of stress drop for moderate to large earthquakes, *J. Geophys. Res.*, *114*, B01310, doi:10.1029/2008JB005821.

Collins, D., and R. Young (2000), Lithological controls on seismicity in granitic rocks, *Bull. Seismol. Soc. Am.*, *90*, 709–723, doi:10.1785/0119990142.

Convers, J. A., and A. V. Newman (2011), Global evaluation of large earthquake energy from 1997 through mid-2010, *J. Geophys. Res.*, *116*, B08304, doi:10.1029/2010JB007928.

Domanski, B., and S. Gibowicz (2008), Comparison of source parameters estimated in the frequency and time domains for seismic events at the Rudna copper mine, Poland, *Acta Geophys.*, *56*(2), 324–343, doi:10.2478/s11600-008-0014-1.

Eshelby, J. (1957), *The Determination of the Elastic Field of an Ellipsoidal Inclusion, and Related Problems*, paper presented at R. Soc. London, vol. A241, pp. 376–396, The Royal Society, London, U. K.

Farrell, J., S. Husen, and R. B. Smith (2009), Earthquake swarm and b-value characterization of the Yellowstone volcano-tectonic system, *J. Volcanol. Geotherm. Res.*, *188*, 260–276, doi:10.1016/j.jvolgeores.2009.08.008.

Hiramatsu, Y., H. Yamanaka, K. Tadokoro, K. Nishigami, and S. Ohmi (2002), Scaling law between corner frequency and seismic moment of microearthquakes: Is the breakdown of the cube law a nature of earthquakes?, *Geophys. Res. Lett.*, *29*(8), 1211, doi:10.1029/2001GL013894.

Ide, S., G. C. Beroza, S. Prejean, and W. Ellsworth (2003), Apparent break in earthquake scaling because of path and site effects on deep borehole recordings, *J. Geophys. Res.*, *108*(B5), 2271, doi:10.1029/2001JB001617.

Ide, S., G. C. Beroza, D. R. Shelly, and T. Uchide (2007), A scaling law for slow earthquakes, *Nature*, *447*, 76–79, doi:10.1038/nature05780.

Igarashi, T., T. Matsuzawa, and A. Hasegawa (2003), Repeating earthquakes and interplate aseismic slip in the northeastern Japan subduction zone, *J. Geophys. Res.*, *108*(B5), 2249, doi:10.1029/2002JB001920.

Iio, Y. (1986), Scaling relation between earthquake size and duration of faulting for shallow earthquakes in seismic moment between 10^{10} and 10^{25} dyne cm, *J. Phys. Earth*, *34*(127–169), 1217–1231, doi:10.1029/JZ072i004p01217.

Kawakata, H., A. Cho, T. Kiyama, T. Yanagidani, K. Kusunose, and M. Shimada (1999), Three dimensional observations of fault formation process in Westerly granite under uniaxial and triaxial conditions by X-ray CT scan, *Tectonophysics*, *313*, 293–305.

Kawakata, H., N. Yoshimitsu, and N. Takahashi (2011), *Development of a Broadband Transducer Assembly Under Triaxial Compressive Conditions*, paper presented at 10th SEGJ Int. Symp., pp. 9–12, Society of Exploration Geophysics of Japan, Tokyo, Japan.

Kwiatek, G., M. Bohnhoff, G. Dresen, A. Schulze, T. Schulte, G. Zimmermann, and E. Huenges (2010), Microseismicity induced during fluid-injection: A case study from the geothermal site at Gross Schoenebeck, North German Basin, *Acta Geophys.*, *58*(6), 995–1020, doi:10.2478/s11600-010-0032-7.

Kwiatek, G., K. Plenkers, and G. Dresen (2011), Source parameters of picoseismicity recorded at Mponeng deep gold mine, South Africa: Implications for scaling relations, *Bull. Seismol. Soc. Am.*, *101*, 2592–2608, doi:10.1785/0120110094.

Kwiatek, G., F. Bulut, M. Bohnhoff, and G. Dresen (2013), High-resolution analysis of seismicity induced at Berlín geothermal field, El Salvador, *Geothermics*, doi:10.1016/j.geothermics.2013.09.008.

Lei, X., K. Kusunose, M. V. M. S. Rao, O. Nishizawa, and T. Satoh (2000), Quasi-static fault growth and cracking in homogeneous brittle rock under triaxial compression using acoustic emission monitoring, *J. Geophys. Res.*, *105*(B3), 6127–6139, doi:10.1029/1999JB900385.

Lockner, D. A., J. D. Byerlee, V. Kuksenko, A. Ponomarev, and A. Sidorin (1991), Quasi-static fault growth and shear fracture energy in granite, *Nature*, *350*, 39–42, doi:10.1038/350039a0.

Madariaga, R. (1976), Dynamics of an expanding circular fault, *Bull. Seismol. Soc. Am.*, *66*, 639–666.

McNutt, S. R. (2005), A review of volcanic seismology, *Annu. Rev. Earth Planet. Sci.*, *33*, 461–491, doi:10.1146/annurev.earth.33.092203.122459.

Mogi, K. (1962), Study of elastic shocks caused by the fracture of heterogeneous materials and their relation to earthquake phenomena, *Bull. Earthquake Res. Inst.*, *40*, 125–173.

Moore, D. E., and D. A. Lockner (1995), The role of microcracking in shear-fracture propagation in granite, *J. Struct. Geol.*, *17*(95–111), 113–114.

Nadeau, R. M., and L. R. Johnson (1998), Seismological studies at Parkfield VI: Moment release rates and estimates of source parameters for small repeating earthquakes, *Bull. Seismol. Soc. Am.*, *88*, 790–814.

Nishizawa, O., T. Satoh, X. Lei, and Y. Kuwahara (1997), Laboratory studies of seismic wave propagation in inhomogeneous media using a laser Doppler vibrometer, *Bull. Seismol. Soc. Am.*, *87*, 809–823.

Oye, V., H. Bungum, and M. Roth (2005), Source parameters and scaling relations for mining-related seismicity within the Pyhasalmi ore mine, Finland, *Bull. Seismol. Soc. Am.*, *95*, 1011–1026, doi:10.1785/0120040170.

Prieto, G. A., P. M. Shearer, F. L. Vernon, and D. Kilb (2004), Earthquake source scaling and self-similarity estimation from stacking P and S spectra, *J. Geophys. Res.*, *109*, B08310, doi:10.1029/2004JB003084.

Scholz, C. H. (1968a), The frequency-magnitude relation of microfracturing in rock and its relation to earthquakes, *Bull. Seismol. Soc. Am.*, *58*, 399–415.

Scholz, C. H. (1968b), Experimental study of the fracturing process in brittle rock, *J. Geophys. Res.*, *73*(4), 1447–1454, doi:10.1029/JB073i004p01447.

Sellers, E. J., M. O. Kataka, and L. M. Linzer (2003), Source parameters of acoustic emission events and scaling with mining induced seismicity, *J. Geophys. Res.*, *108*(B9), 2418, doi:10.1029/2001JB000670.

Somei, K., K. Asano, T. Iwata, and K. Miyakoshi (2014), Source scaling of inland crustal earthquake sequences in Japan using S-Wave coda spectral ratio method, *Pure Appl. Geoph.*, doi:10.1007/s00024-014-0774-2.

Somerville, P. G., K. Irikura, R. Graves, S. Sawada, D. Wald, N. Abrahamson, Y. Iwasaki, T. Kagawa, N. Smith, and A. Kowada (1999), Characterizing crustal earthquake slip models for the prediction of strong ground motion, *Seismol. Res. Lett.*, *70*, 59–80.

Takanami, T., and G. Kitagawa (1988), A new efficient procedure for the estimation of onset times of seismic waves, *J. Phys. Earth*, *36*, 267–290.

Thompson, B. D., R. P. Young, and D. A. Lockner (2006), Fracture in Westerly granite under AE feedback and constant strain rate loading: Nucleation, quasi-static propagation, and the transition to unstable fracture propagation, *Pure Appl. Geophys.*, *163*, 995–1019, doi:10.1007/s00024-006-0054-x.

Urbancic, T. I., and R. P. Young (1993), Space-time variations in source parameters of mining-induced seismic events with $M < 0$, *Bull. Seismol. Soc. Am.*, *83*, 378–397.

Urbancic, T. I., C.-I. Trifu, R. A. Mercer, A. J. Feustel, and J. A. G. Alexander (1996), Automatic time-domain calculation of source parameters for the analysis of induced seismicity, *Bull. Seismol. Soc. Am.*, *86*, 1627–1633.

Utsu, T. (1965), A method for determining the value of b in a formula log n = a - bM showing the magnitude-frequency relation for earthquakes, *Geophys. Bull. Hokkaido Univ.*, *13*, 99–103.

Yamada, T., J. J. Mori, S. Ide, R. E. Abercrombie, H. Kawakata, M. Nakatani, Y. Iio, and H. Ogasawara (2007), Stress drops and radiated seismic energies of microearthquakes in a South African gold mine, *J. Geophys. Res.*, *112*, B03305, doi:10.1029/2006JB004553.

Yanagidani, T., S. Ehara, O. Nishizawa, K. Kusunose, and M. Terada (1985), Localization of dilatancy in Ohshima granite under constant uniaxial stress, *J. Geophys. Res.*, *90*(B8), 6840–6858, doi:10.1029/JB090iB08p06840.

Yoshimitsu, N., H. Kawakata, and N. Takahashi (2009), Broadband P waves transmitting through fracturing Westerly granite before and after the peak stress under a triaxial compressive condition, *Earth Planets Space*, *61*, e21–e24.